Full q-space analysis of x-ray scattering of multilamellar membranes at liquid-solid interfaces

Da-Peng Li, Shu-Xin Hu, and Ming Li*

Beijing National Laboratory for Condensed Matter Physics, Institute of Physics, Chinese Academy of Sciences, Beijing 100080, China

(Received 5 July 2005; revised manuscript received 23 November 2005; published 17 March 2006)

A method for analyzing the x-ray scattering of a stack of phospholipid membranes at the solid-liquid interface in excess water is presented. It is argued that bilayers near the substrate fluctuate less significantly than the ones away from it and, therefore, make a larger contribution to the specular reflection at the low index Bragg peaks. But the diffuse scattering due to thermal fluctuations corrupts the Bragg peaks at high angles so that the specular contribution is not clearly observable. In the midst the specular reflection and the diffuse scattering cannot be separated easily and must be analyzed simultaneously. The height-difference correlation function derived from a modified Caillé theory enables one to simulate the longitudinal and the transverse scans in the same theoretical framework to yield more reliable structural parameters. The theoretical apparatus is successfully applied to the experimental data on DOPC membranes.

DOI: 10.1103/PhysRevE.73.031916 PACS number(s): 87.64.Bx, 61.10.Kw, 87.16.Dg, 87.14.Cc

I. INTRODUCTION

Structural studies of biomembranes are difficult, even for pure lipid bilayers, because of strong thermal fluctuations. Conventional structural analysis has employed the approach of crystallographic x-ray diffraction on multilamellar membranes. However, the biologically relevant lipid membrane arrays are fluidic, having not enough diffraction peaks for crystallographic analysis if fully hydrated. When being deposited on solid substrates, their structure can be easily studied by modern interface-sensitive scattering techniques, which use either synchrotron x rays or neutrons as probes [1–13]. These techniques offer a novel approach to investigate the structure of lipid bilayers. A high degree of orientation makes possible a precise distinction between the scattering vector component normal and parallel to the bilayer, opening up a way to study questions associated with the lateral structure of the bilayers. Furthermore, the solid surface effectively reduces the thermal fluctuations, making it possible to get high resolution electron density profiles, even in fully hydrated states [3,4]. From a technological point of view, solid surfaces may be used in future to manipulate or detect interactions in the biomolecular films deposited on top of them. Biomimetic interfaces and biofunctional surfaces are therefore an active field of interdisciplinary research [4–6]. Many advanced techniques have been invented for the preparation of well-defined, homogeneous and structurally intact membrane systems on solid supports. A particularly simple and low-cost approach to prepare oriented lipid membranes is to spread or to spin coat a solution of lipids onto solid surfaces like silicon, glass, mica, or other flat surfaces [7]. This has promoted much interest in the development of precise and efficient methods to analyze the scattering of x rays or neutrons of such films.

In most published studies on phospholipid multilayers, the integrated Bragg peaks were used for data analysis and the one-dimensional electron density profile $\rho(z)$ is computed by Fourier synthesis using a discrete set of coefficients f_n, as described in, e.g., Refs. [1,14,15]. But, in practice, only a small number of Bragg peaks are observable because of the strong thermal fluctuations of the membranes in fully hydrated state. In such a case, the resulting resolution of $\rho(z)$ is very low, making the Fourier synthesis not attractive. Methods have therefore been developed to use the full range of q_z for data analysis by fitting the continuously measured reflectivity curve to a parametrized model of the density profile [8,16]. In some approaches the rapid falling off of the overall intensity is accounted for by a Lorentz factor q_z^{-1} [9] or q_z^{-2} [10,11,15], while in others the contribution to the scattering by the substrate is explicitly included so that a q_z^{-4} falling off is produced in the framework of Fresnel reflection [4,8] when q_z is small.

In order to determine the true density profile $\rho(z)$ from $f(q_z)$, the effects of thermal and static fluctuations (e.g., due to defects) in the scattering function $S(q_z)$ have to be quantified. Thermal fluctuations are dominant at full hydration when the compressional modulus of the stack is small. To quantify the fluctuation effects and to incorporate them in the reflectivity analysis, one can either treat the layers as discrete [12,13,17] or consider the stack as a continuous elastic medium, described by the classical smectic energy [18] $H=\int_V d^3r\left[\frac{1}{2}B(\partial u/\partial z)^2+\frac{1}{2}K(\nabla_{xy}^2 u)^2\right]$, where $u(x,y,z)$ is the continuum displacement field of the membranes with respect to a perfect lattice, B and K are the bulk moduli for compression and curvature, respectively. K is related to the bending modulus of a single membrane K_c by $K=K_c/d$ and B is related to the compressibility modulus B' in the discrete version of the free energy by $B=B'\cdot d$. The continuum approach is more tractable than the discrete one and yields similar results [9,19]. The model yields a complete description of the fluctuation spectrum, including the dependence of the correlation function on z and on the in-plane distance r.

The solid surface reduces effectively the thermal fluctuations, in particular the large scale undulations so that the height-difference correlation function saturates at a finite value as r becomes large. The measured scattering intensity

*Author to whom all correspondence should be addressed. Email address: mingli@aphy.iphy.ac.cn.

is therefore composed of two parts, i.e., the specular reflectivity and the diffuse scattering [8,20,21]. The true specular component can be obtained by subtracting the offset scan (off-specular background) from the theta-2theta scan, and then fitted to a model with several free Fourier components that define the electron density profile on an absolute scale (see, e.g., [8,11]). But the diffuse scattering contains more information actually [21]. Alternative algorithms have therefore been developed to fit an extensive region of the diffuse scattering data to classical smectic liquid crystal theories to obtain the elastic moduli and the electron density profile [9,21]. But neither of the two methods was able to fully exploit the measured data in **q** space. On the one hand, the diffuse scattering corrupts the specular reflectivity at high q_z. The analysis of the specular reflectivity was limited to a range in which the specular signal can be readily separated from the diffuse scattering. In many cases, only the data up to the third Bragg peak are usable. Sometimes a little osmotic pressure has to be applied to the sample to help to obtain enough data for analysis [22]. On the other hand, the data in the low q_z range were discarded in the diffuse scattering analysis because the specular reflection was not incorporated in the theory [9,21]. The reliability of the analysis relies on the ability to get enough data in the high q_z range. This is sometimes a very hard task, however.

In this work, we present a method that treats the specular reflection and the diffuse scattering in a united way in the framework of a modified Caillé theory reported by us previously [10,23]. The analysis takes into account explicitly the effect of the substrate on thermal fluctuations. According to the theory, the height-difference correlation function saturates at a finite value as r becomes large. This is the reason why specular reflection is observable, even for very thick multilamellar films. With the help of this new correlation function, artificial division of the measured scattering signals into specular and diffuse ones is not necessary any more. The advantage of the method was demonstrated by analyzing the experimental data on DOPC membranes.

II. THEORY

In a Born approximation, the differential cross section for scattering of x rays from a stack of lipid membranes at a solid-liquid interface is the three dimensional Fourier transform of the electron density profile,

$$\frac{d\sigma}{d\Omega} = r_e^2 \left| \int_{-\infty}^{0} dz\, \rho_0 e^{iq_z z} \int_{-\infty}^{+\infty} d^2r\, e^{iq_\parallel r} e^{iqu_0(r)} + \sum_{n=1}^{N} e^{iq_z(n-0.5)d - iq_z \Delta d} \int_{-d/2}^{d/2} dz\, \rho(z) e^{iq_z z} \times \int_{-\infty}^{+\infty} d^2r\, e^{iq_\parallel r} e^{iqu_n(r)} \right|^2, \quad (1)$$

where $r_e = e^2/mc^2$ is the Thompson scattering length of the electron, $q_\parallel$ and q_z are the momentum transfers parallel and perpendicular to the surface, respectively, ρ_0 is the electron density of the substrate, $\rho(z)$ is the electron density profile of a bilayer, N is the total number of the bilayers, and d is the period of the multilayer. Δd in the exponential accounts for the fact that the distance between the solid and the first bilayer might be smaller than the one between the bilayers themselves [24]. If this happens, the multilayer as a whole is shifted by Δd toward the substrate. Note that the electron density profiles are all calculated relative to the medium, which is water in this work. The effective electron density between the substrate and the first layer is zero so that the shift of the multilayer toward the substrate can be mathematically represented by a phase shift of $-iq_z \Delta d$. This phase shift is important only when the film is very thin, for instance, when the film is composed of a few bilayers only. If the overall thickness of the film is large like the one in the present work, this type of shift is not experimentally observable. We will therefore ignore it in the following discussions. For the same reason, we have ignored the SiO_2 layer on the silicon substrate. If needed, it can be simply accounted for by writing the electron density of the substrate $\rho_0(z)$ as a function of depth. The Born approximation is a good one to describe the Fresnel reflectivity only when the longitudinal momentum transfer q_z is larger than the critical one q_c for total external reflection. Fortunately, the reflection below q_c does not affect the accuracy of the calculation of the electron density profiles. Using $f_S = \int_{-\infty}^{0} \rho_0 \exp[iqz] dz$ to represent the reflection of the substrate, and $f_L(q) = \int_{-d/2}^{d/2} \rho(z) \exp[iqz] dz$ the form factor of a bilayer, Eq. (1) can be rewritten in a compact form,

$$\frac{d\sigma}{d\Omega} = r_e^2 \left| \sum_{n=0}^{N} f_n e^{iq_z nd} \int_{-\infty}^{+\infty} d^2r e^{iq_\parallel r} e^{iq_\parallel u_n(r)} \right|^2, \quad (2)$$

where $f_0 = f_S$ and $f_n = f_L \exp[-iq_z d/2 - iq_z \Delta d]$. Assuming that $[u_m(r) - u_n(0)]$ is a Gaussian random variable with the mean of zero and the variance that depends on the distance between the two points, one has

$$\frac{d\sigma}{d\Omega} = r_e^2 \sum_{m,n=0}^{N} f_m f_n^* e^{iq_z(m-n)d} \int_{-\infty}^{\infty} d^2r\, e^{iq_\parallel r} G_{mn}(r) H(r, |m-n|), \quad (3)$$

where $G_{mn}(r) = \exp[-0.5 q_z^2 g_{mn}(r)]$ with $g_{mn}(r) = \langle [u_m(r) - u_n(0)]^2 \rangle$ being the height-difference correlation function. Note that we have explicitly introduced a finite-size factor $H(r, |m-n|)$ to characterize the mosaicity of the film with an average domain size L_r and L_z. Following Dutta and Sinha [15,25], one can write it as $H(r, |m-n|) = \exp[-\pi r^2/L_r^2 - \pi(m-n)^2 d^2/L_z^2]$. In the literature, the correlation function of Caillé type [26] was often used to describe the fluctuations of membranes. However, it is valid for bulk samples only. The suppression of fluctuations by the hard surface must be taken into account for the bilayers supported by a solid. The boundary condition at the flat substrate can be taken into account either by taking the associated surface tension to infinity [27] or by choosing for the fluctuation modes an orthogonal set of eigenfunctions which vanish at the substrate [22,28]. In our previous studies, we obtained a correlation function in a simple and analytical form [10,23],

$$g_{ij}(r) = 2\eta\left[\ln\left(\frac{r^2}{4\lambda^2}\right) - \frac{1}{2}\ln\left(\frac{r^2}{8\lambda z_i}\right) - \frac{1}{2}\ln\left(\frac{r^2}{8\lambda z_j}\right) + E_i\left(\frac{r^2}{4|z_i - z_j|\lambda}\right) - E_i\left(\frac{r^2}{4(z_i + z_j)\lambda}\right)\right], \quad (4)$$

where $\eta = k_B T/(8\pi\sqrt{KB})$, $\lambda = \sqrt{K/B}$ and $E_i(x) = \int_x^\infty t^{-1}e^{-t}\,dt$. Equation (4) can be rewritten as a sum of three parts,

$$g_{ij}(r) = \eta[2g_{ij}^{(\infty)}(r) - g_{ij}^{(i)}(r) - g_{ij}^{(j)}(r)], \quad (5)$$

with

$$g_{ij}^{(\infty)}(r) = 2\gamma_E + Ei\left(\frac{r^2}{4\lambda|z_j - z_i|}\right) + \ln\left(\frac{r^2}{4\lambda^2}\right),$$

and

$$g_{ij}^{(i)}(r) = 2\gamma_E + Ei\left(\frac{r^2}{4\lambda(z_j + z_i)}\right) + \ln\left(\frac{r^2}{8\lambda z_i}\right).$$

Equation (5) has a clear physical meaning that is directly related to the conventional Caillé theory. $g_{ij}^{(\infty)}(r)$ is actually the Caillé correlation function, and $g_{ij}^{(i)}(r)$ represents the suppression of fluctuations of the membranes by a mathematically flat surface.

If the substrate is rough, the membranes near the surface are forced to fluctuate accordingly. Following de Gennes [18], the Fourier spectrum of the fluctuation at a displacement z from the substrate is

$$u(z, q_\parallel) = \exp[-\lambda z q_\parallel^2]u(0, q_\parallel), \quad (6)$$

where $u(0, q_\parallel) = \int u(r, 0)\exp(iq_\parallel r)d^2r$ is the Fourier spectrum of the surface roughness. The height-difference correlation function is thus

$$g_{ij}^{(0)}(r) = 2\int \frac{d^2q_\parallel}{(2\pi)^2} e^{-\lambda(z_i + z_j)q_\parallel^2}|u(0, q_\parallel)|^2(1 - e^{iq_\parallel r}), \quad (7)$$

which should be added to Eq. (4) to fit the experimental data. It should be noted that Eq. (4) is based on a continuum approach of the Caillé model rather than a discrete parametrization of the fluctuation of each bilayer. It is a good approximation when r and Δz are larger than λ. But when the number of bilayers is small or when the lateral momentum transfer $q_\parallel$ is high, the difference between the continuum approach and the accurate discrete result becomes important [9,11]. Fortunately, under most experimental conditions, the lateral momentum transfer that could be reached by a detector is limited, even with the brightest synchrotron radiation sources due to the strong background scattering of water. We will therefore be satisfied with the continuum because it is numerically more efficient than the discrete one.

The effect of the hard wall on the fluctuations of membranes is easily seen in Fig. 1 in which the height-difference correlation functions are depicted for a multilayer with and without the confinement by a substrate. The correlation function of the confined multilayer deviates much from the Caillé scaling because the bilayers have memory for the morphology of the surface of the substrate. Even if the surface of the substrate was mathematically smooth, Eq. (4) ensures that the correlation function saturates rapidly when the membranes are close to the substrate. Therefore, $G_{mn}(r)$ in Eq. (3) does not decay to zero as $r \to \infty$, resulting in specular contributions to the scattering intensity.

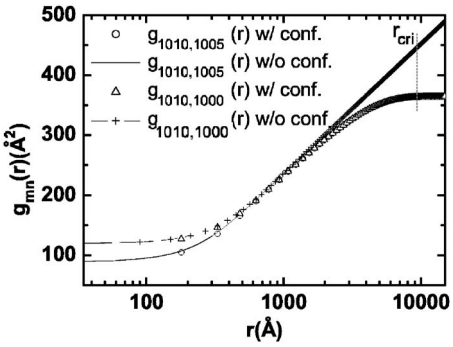

FIG. 1. Examples of height-difference correlation functions for a multilayer with and without confinement by the substrate. The parameters used in the calculation are from the simulation of the sample.

To compare the theory with measured data, one has to integrate Eq. (3) over the solid angle corresponding to the detector's angular acceptance $\Delta\Omega$. That is,

$$I(q) = (I_0/\sin\alpha)\int_{\Delta\Omega} d\Omega(d\sigma/d\Omega). \quad (8)$$

In our experimental setup, the incident wave vector $\mathbf{k}_1$ and the wave vector of scattered radiation $\mathbf{k}_2$ make angles α and β with the interfacial plane, respectively. The factor $\sin\alpha$ converts between the beam's cross-sectional area and its footprint on the sample surface. Let y axis be oriented along the projection of $\mathbf{k}_1$ onto the interfacial plane. The in-plane angle ϕ measures the angle that the projection of $\mathbf{k}_2$ onto the interfacial plane encloses with the y axis. To a good approximation, the components of the momentum transfer $\mathbf{q} = \mathbf{k}_1 - \mathbf{k}_2$ are given in terms of angles α, β, and ϕ as

$$q_x = k\sin\phi,$$

$$q_y = k(\cos\beta - \cos\alpha),$$

$$q_z = k(\sin\beta + \sin\alpha). \quad (9)$$

In our experimental setup, the detector was wide open in the out-of-plane direction to integrate effectively the scattering perpendicular to the scattering plane (along q_x). We assume that the angular acceptance $\Delta\phi$ is large enough so that the scattering at angles $\phi > \Delta\phi/2$ can be neglected, therefore the limits on ϕ integration can be set to $-\infty$ and $+\infty$. This is equivalent to replacing the two-dimensional integration in Eq. (3) by a one-dimensional integration over y only, thus simplifying the numerical evaluation significantly. In the numerical implementation, the most time-consuming part is the double sum of the one-dimensional numerical integral. To speed up the calculation of $G_{mn}(y)$, we built a table for $E_i(x)$. The two exponential integrals $E_i(y^2/4|z_i - z_j|\lambda)$ and $E_i(y^2/4|z_i + z_j|\lambda)$ in Eq. (3) can be obtained by rescaling x and

then making interpolations. The whole computation of the integral and sum was done on an IBM Sp690 computer for about 3 h.

In the conventional longitudinal scans, $\alpha=\beta$. Writing the solid angle element $d\Omega$ as $d\Omega=dq_x\,dq_y/(k^2\sin\beta)$, one can easily show that the intensity $I(0,0,q_z)$ has a prefactor $1/q_z^2$, which is the Lorentz factor for a stack of oriented membranes. Note that in a semikinematical calculation of Salditt *et al.* [8,11], the differential of the electron density profile, i.e., $d\rho(z)/dz$, was used so that the prefactor is $1/q_z^4$ [20]. The two prefactors are therefore equivalent. It is worth pointing out that the overall intensity decays faster than $1/q_z^2$ in the low q_z region because of the scattering of the substrate that is proportional to $1/q_z^2$. The scattering from the substrate dominates the scattering from the multilayer when q_z is small. This is especially true when the film is relatively thin so that the specular scattering is significant. It has been assumed in the above calculation that the width of the sample in the direction of the beam is always larger than the beam's footprint. This is not true at low angles if the sample is not wide enough, in which case the prefactor in Eq. (8) becomes a constant, i.e., $1/\sin\alpha_0$, and the prefactor for the intensity $I(0,0,q_z)$ becomes $1/q_z$ when the incident angle is smaller than α_0 at which the beam's footprint covers the whole sample. An extra factor must also be taken into account, especially at low incident angles. It is the angle dependent absorption term, $\chi(q_z,z)=\exp[16\pi^2(z-D)\nu/\lambda_x^2 q_z]$, where ν is the imaginary component of the index of refraction, λ_x the wavelength of the x rays and D is the total thickness of the film [8]. These two modifications make it inconvenient to numerically calculate the intensity in term of $\mathbf{q}$. We have therefore rewritten Eq. (8) in terms of α and β in the numerical implementation. To do so has one more advantage that the finite resolution of the instrument can be accounted for by direct integrating over the angles $\Delta\alpha$ and $\Delta\beta$, which are the divergence of the primary x-ray beam and the width of the detector's angular acceptance, respectively.

It should be pointed out that the present method is an integration of those reported in Refs. [8,9], each of which is efficient for their respective experimental setup. In Ref. [9], Lyatskaya *et al.* deposited the sample on a cylindrical substrate that was located in the pathway of the incident beam, as in the conventional crystallographic x-ray diffraction approach. The diffraction intensity was imaged by a charge-coupled device (CCD). In such geometry, the intensity recorded by each CCD pixel comes from different values of $\mathbf{q}$ [cf. Eq. (8)], which should be taken into account in the analysis by integrating the theoretical intensity over the appropriate values of $\mathbf{q}$ [21]. Salditt *et al.* [8] used a different approach of structural analysis that arose from the studies on surface and interface of thin solid films [20]; thus the name of interface sensitive scattering method. The samples were deposited on the surfaces of flat solids. The scattering geometry and experimental setup are the same as the ones we will use in the present work (Fig. 2). If the sample is rotated continuously and uniformly with respect to the beam during the data collection by a CCD, as was done in [21], the recorded intensity is the same as the one obtained by Lyatskaya *et al.* [9]. Theoretically, the interface sensitive scattering is sensitive to the difference in electron density across the interfaces in the multilayers [20]. That is why the scattering function is usually expressed in terms of the Fourier transform of the differential of the electron density profile of a layered film. But it is equivalent mathematically to Eq. (1), as has been pointed out many years ago by Sinha *et al.* [20]. Also, the mathematical process of getting Eq. (2) from Eq. (1) proves that the kernels of the two methods are actually equivalent. As compared with the two methods above, our calculation is based on a more accurate correlation function, which accounts for the specular reflectivity in a direct way.

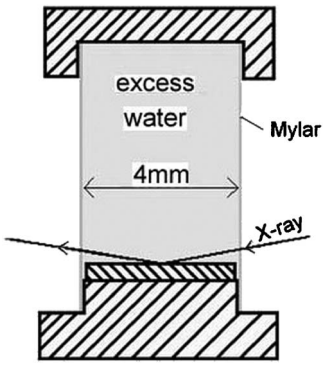

FIG. 2. A sketch of the cross section of the sample cell and the scattering geometry.

We use for the electronic density profile $\rho(z)$ a parametric model adapted from Refs. [29–31], which can provide an absolute scale profile. The hydrophilic headgroup is modeled by two positive Gaussians: one for the phosphate group and the other for the carbonyl group. The ratio of the integrated size of the phosphate group Gaussian to that of the carbonyl group Gaussian is 1.76 according to Ref. [32]. The headgroup displaces a volume V_H, of which 2/3 is water according to computer simulations [33]. It applies a constraint on the sum of the integrated size of the two headgroup Gaussians [30], using the area per lipid molecule given in Refs. [21,34]. The hydrophobic methyl group is represented by a negative Gaussian. The ratio of the volume of the terminal methyl to that of methylene is set to be 1.9 according to Ref. [32]. It constrains the integrated size of the electron deficit of the terminal methyl trough [30]. The electron density of the methylene region is calculated to be $\rho_m=0.287\ e/\text{Å}^3$ according to the headgroup volume $V_H=319\ \text{Å}^3$ and the lipid volume $V_L=1303\ \text{Å}^3$ given in Refs. [29,34,35]. The constant methylene region and water part are smoothly connected by a cosine function with center constrained to lie between the two headgroup Gaussians and with width constrained to the average width of the headgroup Gaussians [36].

III. EXPERIMENTAL RESULTS AND SIMULATIONS

1,2-dioleoyl-sn-glycero-3-phosphocholine (DOPC) was purchased from Avanti Polar Lipids (Birmingham, AL) and used without further purification. The DOPC film was prepared on a hydrophilic Si(001) substrate. The lipid was dissolved in a 1:1(v/v) chloroform:methanol mixture at a con-

centration of 50 mg/ml and pipetted onto the silicon substrate (4×10 mm^2) in a chamber over a period of 12 h. The solution spread spontaneously and the solvent evaporated slowly. The samples were kept in a desiccator for another 24 h at room temperature. It can be estimated that the film contains about two thousand bilayers according to the area per molecule, the total spread area and the volume of the solution pipetted.

The x-ray scattering experiments were performed on the 1W1A beamline at the Beijing Synchrotron Radiation Facility. Monochromatic radiation was selected by a triangular bent Si (220) crystal. The wavelength of the x rays is 1.546 ± 0.002 Å, which was checked by measuring the 004 reflection of a silicon wafer. The vertical and horizontal angular divergences of the focused x-ray beam are 0.02° and 0.08°, respectively. The beam was further confined by a 0.1 mm slit 400 mm before the sample and the scattered beam was confined by two collimating slits. A 0.5 mm slit is located just 10 mm behind the sample. The other is 0.1 mm wide and is located 400 mm behind the sample. A sample cell with two Mylar windows (Fig. 2) is mounted on a five-circle Huber diffractometer. The temperature of the sample cell is controlled by a thermostat with an accuracy of 0.05 °C. The longitudinal scans (also called theta-2theta scans) were performed by keeping the incident angle equal to the exiting angle. The transverse diffuse scattering data were collected by rocking the sample, keeping the angle between the incidence and the reflection fixed.

The sample was equilibrated in excess water [37] for about 2 h before the x-ray measurements. The measurements of a theta-2theta scan and two transverse scans take about 10 and 20 min, respectively. Radiation damage to the sample was checked by measuring a theta-2theta scan again at a different position after performing the last transverse scan. No significant radiation damage was found because the shapes of the first three Bragg peaks in the new theta-2theta scan were almost identical to the previous ones. Nevertheless, care was still taken to avoid exposing the same place of the film to the x rays for more than 30 min. This was done by simple shifting the sample in the direction perpendicular to the x-ray beam. The stability is a little bit problematic because the film was swelling slowly and the top bilayers were peeling off from the film. But this process is extremely slow when the multilayer swells to a stage with an interbilayer distance $d>64$ Å. The fitting procedure showed that the fitting parameters are not sensitive to the total number of bilayers for a wide range of $1500<N<2500$ tested.

Figure 3 shows the x-ray reflectivity of the oriented DOPC film in the fully hydrated state at 30 °C. According to the main phase transition temperature of fully hydrated DOPC [38], the lipid is in the fluid L_α phase in our experiments. The corruption of the higher-order Bragg peaks, indicates the influence of the fluctuations clearly. From the position of the Bragg peaks, one can determine a periodicity of 64.4 Å. The value is a little larger than the spacing d reported by Tristram-Nagle *et al.* [34]. Discussion on the periodicity of the multilayer will be published elsewhere. In this paper we focus only on the theoretical method of getting the structural parameters.

The reflectivity profile contains information of $\rho(z)$, η, and λ. The shape of the Bragg peaks, especially their tails are

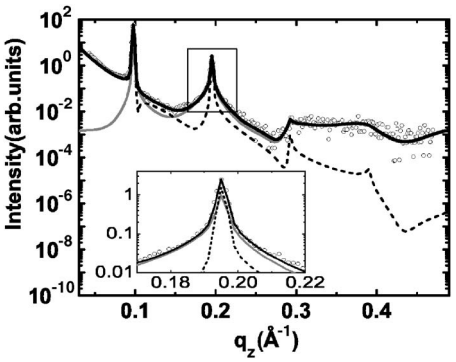

FIG. 3. Longitudinal reflectivity data (symbols) and theoretical calculations (lines) of the multilayer in excess water at 30 °C. The inset shows how the second Bragg peak is constructed. Solid black line: the best fit to the data. Dashed line: calculated specular component. Solid grey line: calculated diffuse component.

mainly determined by η. Paying attention to the overall reflection profile, especially the high q_z part where the specular reflectivity (dashed line in Fig. 3) is weaker than the diffuse scattering (gray line in Fig. 3), one may get satisfactory results of η and $\rho(z)$ by means of the least square fitting. The problem is that one cannot confine the value of η in a narrow range because the discrepancy made by a careless choice of η can be compensated by a modified density profile $\rho(z)$. What is more serious is that the theoretical curve cannot reproduce the data at low q_z, where the specular contribution to the theta-2theta scan is significant. Kučerka *et al.* circumvented this difficulty by combining the analysis of high q_z scattering data from oriented stacks of bilayers with that of low q_z scattering data from extruded unilamellar vesicles [39]. We take a different approach in the present work by calculating the specular reflectivity directly using Eqs. (3)–(7).

The diffuse scattering may help get further constraints on η and λ. One sees that the diffuse scattering profiles in Fig. 4 can be roughly divided into two parts, separated by a critical momentum transfer q_{cri}. The diffuse scattering intensity

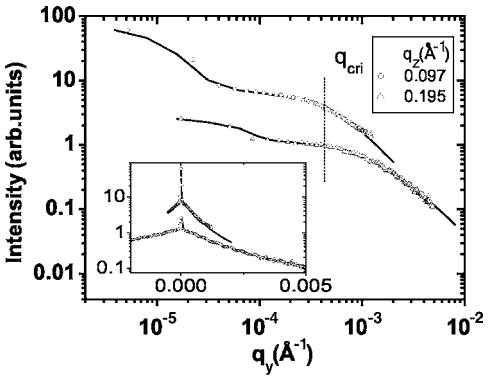

FIG. 4. Transverse diffuse scans of the multilayer in log-log plot at the first Bragg peak (q_z=0.097 Å^{-1}) and the second Bragg peak (q_z=0.195 Å^{-1}), respectively. Inset: the same scans in linear-log plot to emphasize the central specular peak. Symbols are the experimental data. The solid lines are theoretical calculations using the values of λ and η in Table I.

decays faster in large q_y region ($q_y > q_{cri}$) than in small q_y region ($q_y < q_{cri}$). The critical momentum transfer q_{cri} corresponds to the critical length scale r_{cri} ($=2\pi/q_{cri}$) in real space. We learned from the fitting procedure that the diffuse scattering profile below q_{cri} ($\sim 2\pi/r_{cri}$) is mainly due to the geometrical confinement of the substrate on the bilayers. This part is sensitive to $g_{ij}^{(i)}(r)$ in Eq. (5). The diffuse scattering profile above q_{cri} is mainly determined by $g_{ij}^{(\infty)}(r)$ which is just the correlation between the interfaces in bulk liquid crystals. The decay rate in large q_y region is very sensitive to η. We found that the value of η can be relatively easily constrained in a very narrow range by fitting the two diffuse scattering in Fig. 4 simultaneously. In principle, one can also get a good value for λ by fitting the diffuse scattering data if one can separate the specular reflection and the diffuse scattering by carefully checking the transverse scans [10,23]. This has proven to be successful if the central specular peak can be easily identified. However, it is not easy to do so for a stack of lipid membranes in excess water. In the present approach the intensity of the specular reflection is not a free fitting parameter, and the artificial separation is not necessary anymore. One may get satisfactory results of η and λ by means of the least square fitting. But we found that the uncertainty of λ is larger than the uncertainty of η, as in the case of theta-2theta scans.

Now one sees immediately that the most critical part is to obtain the value of λ. It determines at which point a specific correlation function $g_{mn}(r)$ begins to saturate (cf. Fig. 1). It therefore determines the intensity of the specular reflectivity. We have pointed out that neither the theta-2theta scan nor the diffuse scattering alone can confine λ in a very narrow range. But fitting both of them simultaneously would result in a value with smaller uncertainty. The fitting process is as follows. First, λ and η are obtained from the least square fitting of the diffuse scattering profiles. The sensitivity of η to the decay rate of the tails helps to constrain the value of η in a very narrow range, with an uncertainty of about 0.8 Å^2. But λ has a relatively larger uncertainty of about 5 Å. Second, the electron density profile $\rho(z)$ and λ are worked out by simultaneously fitting the theta-2theta scan and the transverse diffuse scans with η being an input parameter. The value of λ obtained from the diffuse scattering is used as an initial guess. Finally, all constraints are released and the parameters are optimized by simultaneously fitting the theta-2theta scan and the transverse diffuse scan.

The continuous line in Fig. 3 shows the best full q_z fit to the theta-2theta scan using the parameters λ and η listed in Table I and the electron density profile $\rho(z)$ in Fig. 5, which agrees well with that published in Ref. [21]. The calculated specular and diffuse components are also depicted to show the advantage of our method. The intensity of the specular component at each Bragg peak is in agreement with that of the corresponding central specular peak of the transverse diffuse scan shown in Fig. 4. The inset in Fig. 3 shows as example how the second Bragg peak is constructed. Although the tails of the Bragg peak are well represented by the diffuse scattering, the very center of the peak is mainly due to the specular reflection. On the other hand, one sees from Fig. 3 that the specular reflection decays very fast so that its contribution to the total scattering is even smaller than that of the diffuse component beyond the third Bragg peak.

TABLE I. Material parameters of DOPC at $T=30$ °C. D_{HH} is the head-head distance across the lipid bilayer. Z_{H1} and Z_{H2} are the positions of the carbonyl group and the phosphate group, respectively. Note that the bending modulus $K_c = K \cdot d$ and the compressibility modulus $B' = B/d$ for the discrete free energy model are listed here.

d (Å)	D_{HH} (Å)	Z_{H1} (Å)	Z_{H2} (Å)	λ (Å)	η (Å^2)	K_c (10^{-13} erg)	B' (10^{12} erg/cm^4)
64.4±0.2	36.3	14.5	18.5	65±2	11.2±0.8	6.3±0.6	3.5±0.4

Listed in Table I are the parameters used in the simulation and the moduli B' and K_c calculated from λ and η. Recently, the values of K_c equal to $8.5\pm0.1\times10^{-13}$ erg at 18 °C [40], $7.3\pm0.4\times10^{-13}$ erg at 30 °C [9] and $8.0\pm0.8\times10^{-13}$ erg at 30 °C [21] have been reported for DOPC, respectively. Our K_c is a little bit smaller than the two values at 30 °C. But it is consistent with the observation that the period of our multilayer is slightly larger than the one reported by Tristram-Nagle *et al.* [34], the reason for which is under study by taking time-resolved measurement of the swelling kinetics of the multilayer. The parameters for domain size are $L_r=1.2$ μm and $L_z=0.2$ μm. We found that the domain size is dependent on the fabrication process and can be increased by annealing the multilayer through repeated hydration and dehydration. We have assumed that the surface of the silicon substrate is self-affine, characterized by a surface roughness σ_0, a lateral correlation length ξ_0, and a Hurst exponent h [20,23]. The power spectrum of the surface fluctuations of the substrate is therefore $|u(0,q_\parallel)|^2 = \int d^2r\, \sigma_0^2 \times \exp(-(r/\xi_0)^{2h}) \exp(iq_\parallel r)$ with the integrand being the correlation function of the surface fluctuations [20,23]. The three parameters for the substrate can be derived by fitting the diffuse scattering of the naked silicon surface, as was done in [23]. They are $\sigma_0=4.4$ Å, $\xi_0=800$ Å, and $h=0.4$, respectively. The power spectrum, $|u(0,q_\parallel)|^2$, calculated according to these parameters is small as compared to that of the intrinsic fluctuations of the membranes. $g_{ij}^{(0)}(r)$ is therefore not a significant term for the silicon-supported multibilayer in this work. However, it should not be ignored when the multi-

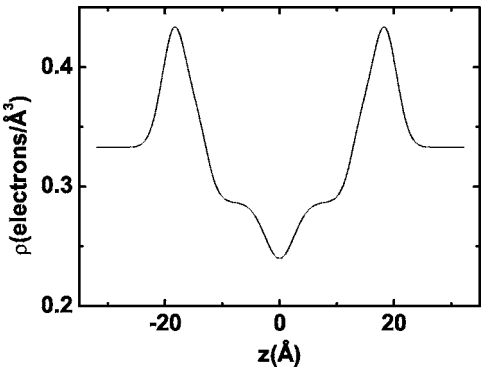

FIG. 5. Electron density profile $\rho(z)$ corresponding to the simulation in Fig. 3.

bilayer is composed of only a few bilayers or when the multibilayer is deposited on a very rough surface, e.g., a glass surface. Ignoring the effect of the surface roughness in the later two cases would result in a wrong value of λ, although the parameter η would be less significantly affected.

We now show how one can give a rough estimate for an appropriate initial value of λ in the least square fitting of the diffuse scattering profiles. According to Eq. (6) one can define an effective vertical correlation length $\xi_\perp = 1/(\lambda q_\parallel^2)$. Supposing that q_{cri} is the critical momentum transfer of the interfacial fluctuations below which the vertical correlation $\xi_\perp$ is beyond the total thickness of the film, one has $\lambda \approx 50$ Å according to the estimated total thickness of the film and the critical momentum transfer $q_{cri} \sim 0.0004$ Å^{-1} read from Fig. 4. The corresponding critical length in real space r_{cri} is about 1.5 μm, which is just slightly larger than the one marked in Fig. 1, which says that the correlation function $g_{1010,1000}(r)$ between two layers near the center of the sample begins to saturate at 1.0 μm.

IV. SUMMARY

Solid-supported stacks of bilayers are very important for structural studies of lipids especially in the biologically relevant, fully hydrated L_α phase. The substrate suppresses the thermal fluctuations in lipid multilayers. We have presented an analysis method for the x-ray scattering of such multilayers based on a theory, which takes into account the effect of the substrate. The advantage of the method is that the scattering signals in the full q_z range are analyzed without partitioning the specular and the diffuse components artificially.

We have emphasized that, for the x-ray scattering of a stack of membranes supported by a solid, the specular reflection dominates in the low q_z range, but the diffuse scattering does so in the high q_z range. It is in most cases difficult to distinguish one from the other by just looking at the experimental data. But in recent theories, either the specular reflection or the diffuse scattering was used independently for analysis. Having their own excellence, those treatments used only a part of the available data. On the contrary, the two parts are united in our theory through the reasonable consideration of the effect of the substrate. The data in the measured q_z range are fully exploited. This method brings promise to provide more reliable material parameters and structural information of lipid bilayer in fully hydrated L_α phase.

ACKNOWLEDGMENTS

This work was financially supported by the National Natural Science Foundation of China (Grants No. 10325419 and No. 10334100) and by the Beijing Synchrotron Radiation Laboratory.

[1] J. Katsaras, Biochem. Cell Biol. **73**, 209 (1995).
[2] S. Tristram-Nagle and J. F. Nagle, Chem. Phys. Lipids **127**, 3 (2004).
[3] T. Salditt, Curr. Opin. Colloid Interface Sci. **5**, 19 (2000).
[4] T. Salditt, Curr. Opin. Struct. Biol. **13**, 467 (2003).
[5] L. Yang and H. W. Huang, Science **297**, 1877 (2002).
[6] K. Hristova, W. C. Wimley, V. K. Mishra, G. M. Anantharamiah, J. P. Segrest, and S. H. White, J. Mol. Biol. **290**, 99 (1999).
[7] M. Seul and P. Eisenberger, Phys. Rev. A **39**, 4230 (1989).
[8] T. Salditt, C. Li, A. Spaar, and U. Mennicke, Eur. Phys. J. E **7**, 105 (2002).
[9] Y. Lyatskaya, Y. F. Liu, S. Tristram-Nagle, J. Katsaras, and J. F. Nagle, Phys. Rev. E **63**, 011907 (2000).
[10] S. X. Hu, X. H. Li, Q. J. Jia, Z. H. Mai, and M. Li, J. Chem. Phys. **122**, 124712 (2005).
[11] C. H. Li, D. Constantin, and T. Salditt, J. Phys.: Condens. Matter **16**, S2439-S2453 (2004).
[12] R. Holyst, Phys. Rev. A **44**, 3692 (1991).
[13] N. Lei, C. R. Safinya, and R. F. Bruinsma, J. Phys. II **5**, 1155 (1995).
[14] A. E. Blaurock, Biochim. Biophys. Acta **650**, 167 (1982).
[15] R. Zhang, R. M. Suter, and J. F. Nagle, Phys. Rev. E **50**, 5047 (1994).
[16] G. Pabst, M. Rappolt, H. Amenitsch, and P. Laggner, Phys. Rev. E **62**, 4000 (2000).
[17] V. P. Romanov and S. V. Ul'yanov, Phys. Rev. E **66**, 061701 (2002).
[18] P. G. de Gennes and J. Prost, *The Physics of Liquid Crystals*, 2nd ed. (Clarendon, Oxford, 1993).
[19] A. Poniewierski and R. Holyst, Phys. Rev. B **47**, 9840 (1993).
[20] S. K. Sinha, E. B. Sirota, S. Garoff, and H. B. Stanley, Phys. Rev. B **38**, 2297 (1988).
[21] Y. F. Liu and J. F. Nagle, Phys. Rev. E **69**, 040901(R) (2004).
[22] D. Constantin, U. Mennicke, C. Li, and T. Salditt, Eur. Phys. J. E **12**, 283 (2003).
[23] X. H. Li, M. Li, and Z. H. Mai, J. Phys. Chem. B **108**, 8338 (2004).
[24] J. F. Nagle and J. Katsaras, Phys. Rev. E **59**, 7018 (1999).
[25] P. Dutta and S. K. Sinha, Phys. Rev. Lett. **47**, 50 (1981).
[26] A. Caillé, C. R. Acad. Sci. **274B**, 891 (1972).
[27] A. N. Shalaginov and V. P. Romanov, Phys. Rev. E **48**, 1073 (1993).
[28] D. K. G. de Boer, Phys. Rev. E **59**, 1880 (1999).
[29] M. C. Wiener, R. M. Suter, and J. F. Nagle, Biophys. J. **55**, 315 (1989).
[30] J. F. Nagle and M. C. Wiener, Biophys. J. **55**, 309 (1989).
[31] J. F. Nagle, R. Zhang, S. Tristram-Nagle, W. J. Sun, H. I. Petrache, and R. M. Suter, Biophys. J. **70**, 1419 (1996).
[32] R. S. Armen, O. D. Uitto, and S. E. Feller, Biophys. J. **75**, 734 (1998).
[33] S. E. Feller, D. Yin, R. W. Pastor, and A. D. MacKerell, Biophys. J. **73**, 2269 (1997).
[34] S. Tristram-Nagle, H. I. Petrache, and J. F. Nagle, Biophys. J. **75**, 917 (1998).
[35] W. J. Sun, R. M. Suter, M. A. Knewtson, C. R. Worthington, S.

Tristram-Nagle, R. Zhang, and J. F. Nagle, Phys. Rev. E **49**, 4665 (1994).
[36] S. Tristram-Nagle, Y. F. Liu, J. Legleiter, and J. F. Nagle, Biophys. J. **83**, 3324 (2002).
[37] J. Katsaras, Biophys. J. **73**, 2924 (1997).
[38] P. G. Barton and F. D. Gunstone, J. Biol. Chem. **250**, 4470 (1975).
[39] N. Kučerka, Y. F. Liu, N. J. Chu, H. I. Petrache, S. Tristram-Nagle, and J. F. Nagle, Biophys. J. **88**, 2626 (2005).
[40] W. Rawicz, K. C. Olbrich, T. McIntosh, D. Needham, and E. Evans, Biophys. J. **79**, 328 (2000).